Int. J. Heat Mass Transfer. Vol. 34, No. 2, pp. 559–572, 1991
Printed in Great Britain

0017-9310/91 $3.00 + 0.00
© 1991 Pergamon Press plc

Simulation of the mass transfer behaviour of individual gas bubbles undergoing fast chemical stripping using the jet stream model

F. XAVIER MALCATA
Escola Superior de Biotecnologia, Universidade Católica Portuguesa,
Rua Dr. António Bernardino de Almeida, 4200 Porto, Portugal

(*Received* 13 *October* 1989 *and in final form* 23 *April* 1990)

Abstract—The mass transfer of solute from a dilute gaseous mixture during bubble formation at the tip of a submerged nozzle in the presence of an instantaneous chemical reaction on the liquid side is simulated via a two-parameter model. This mechanistic model is developed from the general mass balance of solute by introducing a number of physically reasonable assumptions coupled with carefully checked mathematical approximations. Using data reported elsewhere, parameter estimates are found and a statistical analysis of their significance is presented. Experimental evidence is predicted much better than via other theoretical models. The analysis reported is useful for the preliminary design of industrial sparging vessels because most of the solute removal occurs during bubble growth.

1. INTRODUCTION

THE REMOVAL of a solute from a gaseous mixture via dispersion in a suitable liquid phase has motivated a number of theoretical and experimental studies because of its potential for chemical engineering applications. Of particular interest is the stripping of a dilute solute from a gaseous phase accompanied by a chemical reaction within the liquid phase. This interest can be attributed to the fact that (i) the mass transfer rates are extremely enhanced with respect to the physical absorption counterpart, and (ii) the gaseous impurity removed can be readily converted to a different chemical species with hopefully less disposal problems. When the solute being transported undergoes a very fast, irreversible reaction upon contact with the liquid then the liquid film where the reaction takes place tends to a plane of negligible thickness. This plane lies on the interface whenever the liquid reactant exists in large excess [1]. In this situation the resistance to mass transfer arising from the liquid side vanishes, so the prediction of the fractional removal of solute from the gas phase virtually becomes a single-phase problem. The condition of gas phase diffusional control is approximately valid for a number of systems of industrial significance (e.g. removal of ammonia from effluent mixtures of NH_3/air via acidic solutions and stripping of H_2S from dilute gas streams using strong aqueous alkalis [2]).

It is common practice to account for the mass transfer process in bubbling operations by means of a single overall coefficient. It has been pointed out, however, that the bubble formation stage accounts for most of the mass transfer under the assumption of an instantaneous reaction occurring on the liquid side [3]. Hence the contributions for mass transfer arising from the bubble rise stage and the bubble staying either in the surface foam or in the vessel headspace after breakup are not important for the operating conditions of industrial interest. The attempt to develop a mechanistic model for the molecular transport of mass during bubble growth of individual bubbles is, therefore, of both academic interest and industrial significance, provided that sparged vessels with sufficiently separated bubbling orifices are employed [4].

During the growth stage, the behaviour of the bubble can be approached as a particular case of the more general problem of mass transfer in the presence of a mobile interface. The fundamental interpretations of this phenomenon can be divided into two major groups according to the underlying physicochemical rationale: (i) static models, where the growing interface is simulated as a deformable surface, with all gas elements on the surface sharing the same residence time [5–11]; and (ii) dynamic models, where the growing interface is assumed to consist of gas elements with different ages, which keep their absolute position [12, 13] or slide continuously (thus spanning the surface of the bubble according to a toroidal path) [14, 15].

In this paper, a new mechanistic model aimed at the prediction of the mass transfer rates of a solute from growing bubbles in the presence of an instantaneous reaction on the liquid side is introduced and discussed. The model assumes the circulation within the bubble to result from a confined gaseous jet originated at the tip of the submerged nozzle. A number of physical and algebraic simplifications are made in order to produce mathematical expressions which are

NOMENCLATURE

A_{des} area of gas elements from which solute was ever removed at the surface of the bubble
A_{surf} actual surface area of bubble
C_{bub} concentration of solute in the bulk of the bubble
C^*_{bub} normalized concentration of solute, C_{bub}/C_{in}
$C^*_{bub,crt}$ concentration of solute in the bulk of the bubble at a critical point
C_{in} concentration of solute at the inlet gas stream
$\mathscr{D}_{gas}$ diffusivity of solute in the gas phase
g acceleration of gravity
J total momentum of jet in the longitudinal direction, $2\pi\rho_{gas}\int_0^\infty U^2(x,\psi)\psi\,d\psi$
P_n nth order polynomial
Q_{gas} volumetric flow rate of gas
R_{bub} radius of the bubble
R_{noz} radius of the nozzle
t time elapsed since bubble birth
t^* dimensionless time, t/t_{fin}
t_i time at which the gas element arrives at the surface of the bubble
t_i^* dimensionless time, t_i/t_{fin}
$t_{i,app}$ approximate value of t_i using approximation I
$t^*_{i,app}$ dimensionless time, $t_{i,app}/t_{fin}$
$T_{j,n}$ jth order term of the nth order polynomial, $T_{j,n}(\Xi) := 6^{-n}\tau_{j,n}\Xi^j$, $1 \leqslant j \leqslant n$
t_f time at which the gas element leaves the surface of the bubble
t_f^* dimensionless time, t_f/t_{fin}
t_{fin} time of bubble release from the nozzle
$(t_f^*-t_i^*)_{app}$ approximate value of $(t_f^*-t_i^*)$ using approximation IV
U longitudinal component of the gas velocity within the jet
V radial component of the gas velocity within the jet
V_{bub} volume of the bubble
v_{ren} rate of surface displacement due to the natural surface renewal
x longitudinal distance to the nozzle opening
y radial distance to the axis of symmetry of the jet.

Greek symbols

α_1 constant of proportionality
α_2 constant of proportionality
α_3 constant of proportionality
ζ dimensionless radial coordinate, $\sqrt{(3J\rho_{gas})}y/4\sqrt{\pi\mu_{gas}\Theta\{U(x=0,\zeta=0)\}}x$
Θ corrective function accounting for the extra turbulence within a constrained jet relative to the free jet counterpart
θ new form of parameter ξ after the second reparametrization is carried out, ξ
ϑ dimensionless constant, $256\cdot 191^{2/3}\pi^{9(1-\xi)/3}\mu_{gas}^2 Q_{gas}^{(15\xi-11)/5}R_{noz}^{4-6\xi}/756^{2/3}\Phi\rho_{gas}^2 g^{2/5}$
λ exponent used for power transformation of the data or response
μ viscosity
ν new form of parameter Φ after the second reparametrization is carried out, $1/\Phi^{0.4867}$
Ξ dimensionless parameter, $189\cdot 6112^{1/2}\cdot 191^{1/3}\cdot 4^{1/6}\pi^{(9\xi-11)/6}\cdot(\Phi\mathscr{D}_{gas})^{1/2}\rho_{gas}g^{1/10}Q_{gas}^{(8-15\xi)/10}R_{noz}^{3\xi-2}/764\cdot 21^{1/2}\cdot 168^{1/3}\cdot 3^{1/6}\mu_{gas}$
ξ dimensionless exponent of power dependence of Θ on $U(x=0,\zeta=0)$
ρ_{gas} mass density of gas phase
τ numerical coefficient independent of parameter Ξ
Φ lumped proportionality constant, $\alpha_1\alpha_2^3$
ϕ new form of parameter Φ after the first reparametrization is carried out, $\ln\{\Phi\}$
φ new form of parameter ξ after the first reparametrization is carried out, $\ln\{15\xi/8\}$
ψ dummy variable of integration.

easier to tackle; all mathematical approximations are checked a posteriori. The model contains two parameters, which are fitted to experimental data made available elsewhere [3]. Both adjustable parameters can be ascribed simple physical meanings. The fit is checked for validity of the underlying assumptions on the variance of the errors, and the model is tested for adequacy of its functional and parametric form. The range where extra experimental data should be obtained for further refinement of the parameter estimates is also reported.

2. DERIVATION OF THE MATHEMATICAL MODEL

The exact description of the mass transfer of solute from the bulk of a gas bubble towards the liquid/gas interface during bubble formation at a nozzle tip is extremely complex due to the stochastic behaviour of the fluid elements within the bubble. This behaviour arises from the eddies generated by the interaction of the inlet jet stream with the existing gas in a confined space. Even with negligible liquid resistance to mass

transfer and negligible free convection within the bubble, the exact solution of the differential mass balance for the solute would require an a priori knowledge of the velocity field within the gaseous phase [16]. Although this velocity field will be known in detail sometime in the near future, the solution of the corresponding differential mass balance will be reached only at the expense of much involved numerical approaches. These approaches are expected to be too lengthy for widespread application, and too complex to provide a useful insight to the mass transfer phenomena.

A possible way to overcome the aforementioned problem consists of taking a number of simplifying postulates on the hydrodynamic pattern within the bubble to be valid. The main assumptions considered in this communication are listed next: (i) the bubble is considered to retain perfect spherical shape, so all geometrical properties of a sphere apply; (ii) isothermal and isobaric conditions of operation are assumed throughout, so temperature and pressure are dropped out as disturbances; (iii) the solute exists in the gaseous phase at a very dilute level, so the convective term in Fick's first law arising from bulk flow is negligible, and the inlet and outlet volumetric flow rates of gas are virtually equal; (iv) the bulk of the bubble is a perfectly stirred pool, so no concentration gradients can develop within the bubble core; (v) gas elements previously existing in the bulk of the bubble are thrown at random to the bubble surface due to the interaction with the jet generated at the inlet nozzle; (vi) the actual area of the bubble surface grows at the expense of gas elements at the vicinity of the point of impact of the jet with the liquid/gas interface (forced surface renewal); (vii) all gas elements thrown to the surface undergo plug flow as they are displaced along the bubble shell, from the impact point until the wake of the bubble is reached, with a given rate of surface displacement, v_{ren} (natural surface renewal); (viii) the gas elements returned to the bulk of the bubble at the neighbourhood of the nozzle are replaced by an equivalent amount of gas elements with bulk composition at the jet impact point; (ix) the mass flux of solute is essentially unidimensional and normal to the surface of the bubble at each point, so no mass transfer between adjacent gas elements on the surface is allowed; (x) the solvent in the gaseous phase and all components in the liquid phase are stagnant as far as the gas phase is concerned; and (xi) the rate of transfer of solute at each point on the surface is obtained from the classical penetration theory under the assumption of unsteady-state conditions in a semi-infinite medium [17, 18], so any change in the concentration of solute in the immediate vicinity of the inner surface of the outer gas shell due to back diffusion towards the bulk of the bubble does not affect the concentration profile in the neighbourhood of the outer surface of the gas shell. The two mechanisms of surface renewal on the gas side assumed above are depicted in Fig. 1.

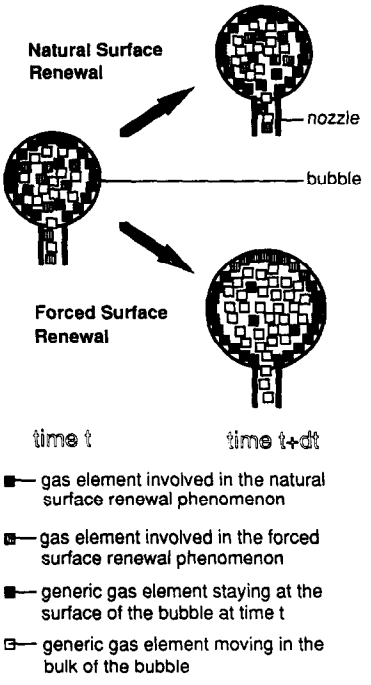

FIG. 1. Schematic representation of the two mechanisms of surface renewal postulated for the period of bubble birth and growth at the tip of a submerged nozzle.

According to the foregoing postulates, the mass balance for the solute can then be written as [15]

$$Q_{gas}C_{in} = Q_{gas}\left(C_{bub} + t\frac{dC_{bub}}{dt}\right) + 2\sqrt{\left(\frac{\mathscr{D}_{gas}}{\pi}\right)}\int_0^{A_{surf}(t)} \frac{C_{bub}(\psi)}{\sqrt{(t-t_i(\psi))}}\,d\psi. \quad (1)$$

The term on the left-hand side of the above equation represents the inlet molar rate of solute. The first term on the right-hand side corresponds to the molar rate of accumulation of solute within the bubble, i.e. $d(V_{bub}\cdot C_{bub})/dt$ where $V_{bub} = Q_{gas}\cdot t$. The integral term on the right-hand side accounts for the molar rate of solute disappearance by chemical reaction from all gas elements residing at the interface; since no accumulation is permitted at the interfacial plane, this kinetic rate must equal the rate of transport of solute by molecular diffusion across the gas layer near the surface of the bubble. The foregoing integro-differential equation must satisfy the following initial condition:

$$@\ t = 0, \quad C_{bub} = C_{in}. \quad (2)$$

For the gas elements that hit the bubble surface at time t_i, removal of solute takes place until time $t_f(t_i)$. During the time period $(t_f - t_i)$, the gas element slides along the surface with decreasing v_{ren}, spanning an area equal to the actual area of the bubble surface at time t_i. This statement is mathematically equivalent to writing [14]

$$A_{surf}(t_i) = \int_{t_i}^{t} v_{ren}(\psi)\, d\psi. \quad (3)$$

The rate of variation of the area occupied by gas elements on the surface undergoing stripping of solute, dA_{des}/dt, can be obtained by summing up the rate of variation of the bubble surface area due to forced renewal, dA_{surf}/dt, and the elementary variation of the area due to natural surface renewal, v_{ren}, according to

$$\frac{dA_{des}(t)}{dt} = \frac{dA_{surf}(t)}{dt} + v_{ren}(t). \quad (4)$$

If the bubble had infinite size, the flow pattern of the gas within the bubble would approach that of a free, infinitesimally narrow jet. The efflux of a jet from a small circular orifice that mixes with the surrounding stagnant fluid can be studied via the application of the boundary layer theory [19]. Disregarding small velocities of flow, it is found that the jet becomes completely turbulent at a short distance from the point of discharge. Owing to turbulence, the emerging jet carries with it some of the surrounding fluid which was originally at rest because of the friction developed on its periphery. The jet spreads outwards in the downstream direction owing to the influence of friction, whereas its velocity in the centre decreases in the same direction [19]. Although the flow tends to become turbulent, one will use the exact mathematical solution for the laminar case as a basis for the general derivation, since both laminar and turbulent flow are described by similar differential equations. Consistency can be maintained throughout if suitable multiplicative correction factors are introduced in order to allow for turbulence [19]. The case of a compressible circular laminar jet was evaluated elsewhere [20]; one will not follow it here, however, because the characteristic values of the Mach number associated with the jet for the interesting ranges of operation are much smaller than unity.

One adopted a system of spatial coordinates with its origin in the nozzle opening, with its axis of abscissae coinciding with the jet axis, and with its ordinate denoting the radial distance with respect to the jet axis. The solution for the free circular jet problem was first obtained by Schlichting [21]. Similarity arguments have been employed to relate the velocity profiles in the free jet and in the constrained jet within a bubble. Since the width of the jet is proportional to the longitudinal position under turbulent conditions [19], one can account for the finite character of common bubbles by including in the proportionality constant, Θ, a contribution from the driving force for the mixing pattern within the bubble (i.e. the inlet velocity of the gas, $U(x = 0, \zeta = 0)$). The result for the longitudinal and radial components of the velocity of the jet are thereby obtained to be

$$U(x,\zeta) = \frac{3J}{8\pi\sqrt{\mu_{gas}}\left(1+\frac{\zeta^2}{4}\right)^2 \Theta\{U(x=0,\zeta=0)\}x} \quad (5)$$

and

$$V(x,\zeta) = \frac{\sqrt{(3J)}\left(\zeta+\frac{\zeta^3}{4}\right)}{4\sqrt{(\pi\rho_{gas})}\left(1+\frac{\zeta^2}{4}\right)^2 \Theta\{U(x=0,\zeta=0)\}x} \quad (6)$$

respectively.

Inspecting the functional form of the correlations for the Fanning friction factor on the Reynolds number [16], remembering that the pressure drop within a confined fluid is a measure of the degree of turbulence inside that phase, and assuming that analogy exists between the form of the correlations for the case of infinite cylindrical and finite spherical geometry, one finds that the function $\Theta\{U(x = 0, \zeta = 0)\}$ should be tentatively expressed as

$$\Theta\{U(x=0,\zeta=0)\} = \alpha_1 \left(\frac{Q_{gas}}{\pi R_{noz}^2}\right)^{\xi} \quad (7)$$

where ξ is an arbitrary non-negative parameter. Owing to the assumption of a constant pressure along the gas path, the flux of momentum in the direction of x is constant. If one assumes in addition that the velocity profile at the nozzle tip is uniform, then the total momentum of the free jet is given by

$$J = \frac{\rho_{gas} Q_{gas}^2}{\pi R_{noz}^2}. \quad (8)$$

For conditions approaching constant flow rate of gas through a submerged nozzle, a simple relationship derived by equating the buoyant force to the inertia force of the liquid that fits experimental data reasonably well was suggested by Davidson and Schüller [22]. Such a predictive expression can be formulated as follows:

$$t_{fin} = \frac{191\sqrt{Q_{gas}^{1/5}}}{168 g^{3/5}}. \quad (9)$$

The inlet gas stream moves across the bubble core and eventually impinges the bubble surface at the neighbourhood of the intercept of the axis of symmetry of the nozzle with the gas/liquid interface. Some of the pressure–volume work of the entering stream is converted into surface energy; the gas elements more likely to occupy the extra amount of interface available are gas elements directly generated from the jet stream after thorough mixing with the bulk gas. The remaining gas elements that are not allowed to participate in the formation of an extended interface in the vicinity of the stagnation point may either rebound back or slide along the bubble surface. The former phenomenon is less likely to occur than the latter because the high longitudinal component of the jet stream opposes the rebound tendency. The exact solu-

tion of the Navier–Stokes equations for the latter axisymmetric flow does not exist, but the closed form solutions reported by Homann [23] and Schlichting [19] for the case of a rotationally symmetric flow at a stagnation point suggest that frictional forces should retard the motion of fluid in a thin layer near the interface (where the non-slip condition is assumed to be satisfied [24]). If a parabolic velocity profile develops in the boundary layer close to the interface, and if unidirectional flow is assumed for the sake of simplicity, the differential mass balance to the solute assumes the form of a pseudo-Purday problem [25, 26], for which an analytical solution exists in the form of an infinite series. Inspection of the concentration profiles for the case of the laminar flow and plug flow [27] confirms that very little difference exists between them for the range of Peclet numbers of industrial interest (i.e. $0.1 \leqslant Pe \leqslant 10$). Therefore, the assumption of a plug flow on the bubble outer gas shell is operationally and mathematically justified.

The rate of surface renewal, v_{ren}, should be proportional (i) to the longitudinal velocity at the point of impact of the jet with the surface of the bubble (because this is a measure of the driving force for the movement of surface gas elements at this point), and also proportional (ii) to the local variation of the radial velocity of the jet in the axial direction at the point where the jet impinges the gas/liquid interface (because this is a measure of the entrainment of the gas jet in the radial direction at the neighbourhood of the same point). This statement can be mathematically expressed as

$$v_{ren} = \alpha_2 U(x = 2R_{bub}, \zeta = 0)\left(\frac{\partial V}{\partial y}\right)_{x = 2R_{bub}, \zeta = 0}. \quad (10)$$

The resulting expression for v_{ren} can then be obtained from equations (5) to (9) to be

$$v_{ren} = \frac{63\pi^{3(\xi-1)}\Phi g^{3/5}\rho_{gas}^2 Q_{gas}^{(14-15\xi)/5} R_{noz}^{6\xi-4}}{6112\mu_{gas}^2 t^*}. \quad (11)$$

Using equation (11) coupled with the geometrical properties of the bubble, equation (3) becomes

$$3\vartheta t_i^{*2/3} = \ln\left\{\frac{t_f^*}{t_i^*}\right\}. \quad (12)$$

The above equation cannot be explicitly solved for $t_i^*(t_f^*)$. However, if $(t_i^*/t_f^*)^{2/3}$ and $\ln(t_f^*/t_f^*)$ are expanded as a Taylor series about t_f^*, and if one assumes that t_i^* is not much smaller than t_f^*, then good accuracy is obtained when truncation is made after the linear terms (approximation I). Applying this mathematical artifact, equation (12) becomes

$$t_i^* \approx t_{i,app}^* = \frac{(1-\vartheta t_f^{*2/3})t_f^*}{1+2\vartheta t_f^{*2/3}}. \quad (13)$$

In order to account for the high rates of stripping experimentally observed, equation (4) should in principle reduce to (approximation II)

$$\frac{dA_{des}}{dt} \approx v_{ren}(t). \quad (14)$$

If $C_{bub}(\psi)/\psi$ does not change appreciably from t_i^* to t^*, then one can state that (approximation III)

$$\frac{C_{bub}(\psi)}{\psi} \approx \frac{C_{bub}(t^*)}{t^*}. \quad (15)$$

Substitution of equations (11), and (13)–(15) in equation (1) gives

$$1 = C_{bub}^* + t^*\frac{dC_{bub}^*}{dt^*} + \frac{\Xi C_{bub}^*}{12t^*}\int_{t_i^*(t^*)}^{t^*}\frac{d\psi}{\sqrt{(t^*-\psi)}}. \quad (16)$$

Equation (16) can be made equivalent to

$$1 = t^*\frac{dC_{bub}^*}{dt^*} + C_{bub}^*\left(1 + \frac{\Xi}{6t^{*1/6}}\right) \quad (17)$$

provided that equation (13) is first approximately transformed to (approximation IV)

$$t_f^* - t_i^* \approx (t_f^* - t_i^*)_{app} = 3\vartheta t_f^{*5/3}. \quad (18)$$

Applying the integrating factor rule to equation (17), one obtains

$$C_{bub}^*(t^*) = \frac{\int \exp\left\{-\frac{\Xi}{\psi^{1/6}}\right\} d\psi}{t^* \exp\left\{-\frac{\Xi}{t^{*1/6}}\right\}}. \quad (19)$$

In order to avoid numerical integration, one can resort to expressing equation (19) as an infinite combination of elementary functions. This can be done by expanding $\exp\{-\Xi t^{*-1/6}\}$ as a Taylor series about $t^* = 1$. Using the dimensionless counterpart of equation (2) coupled to some algebraic manipulation, one finally obtains

$$C_{bub}^*(t^*) = \frac{1 + \sum_{n=1}^{\infty}\frac{(-1)^{n+1}((1-t^*)^{n+1}-1)P_n(\Xi)}{t^*(n+1)!}}{1 + \sum_{n=1}^{\infty}\frac{(-1)^n(1-t^*)^n P_n(\Xi)}{n!}} \quad (20)$$

where the nth degree real polynomial is defined by the following recursive relation:

$$P_1(\Xi) = T_{1,1} = \frac{\Xi}{6}$$

$$P_n(\Xi) = \sum_{j=1}^{n-1}\left(\frac{\Xi}{6} + 1 - n - \frac{j}{6}\right)T_{j,n-1}(\Xi), \quad n \geqslant 2. \quad (21)$$

The coefficients for the first polynomials $P_n(\Xi)$ are

Table 1. Coefficients $\tau_{j,n}$ of the polynomials $P_n(\Xi)$ for each order j such that $1 \leqslant j \leqslant n$, for degree n such that $1 \leqslant n \leqslant 6$

			n			
j	1	2	3	4	5	6
1	1					
2	−7	1				
3	91	−21	1			
4	−1729	511	−42	1		
5	43225	−15015	1645	−70	1	
6	−1339975	523705	−69300	4025	−105	1

compiled in Table 1. Inspection of the size of the coefficients as n increases allows one to find that, for fairly large values of parameter Ξ coupled with lower values of t^*, convergence of the infinite series in equation (20) is slow. Therefore, quadruple precision was required for the FORTRAN code implemented in order to get accurate results. The variation of $C^*_{bub}(t^* = 1)$ with respect to Ξ as given by equation (20) is represented in Fig. 2. It is remarkable that $C^*_{bub}(t^* = 1)$ becomes a simple power function of Ξ at large values of Ξ (say, greater than 10^2) expressed by

$$\lim_{\Xi \to \infty} C^*_{bub}(t^* = 1, \Xi) = \frac{5.0396}{\Xi^{0.9733}}. \tag{22}$$

This asymptotic behaviour can be taken advantage of during the fit of the theoretical model because the experimental data available lie in this range.

The concentration of solute in the bulk of the bubble does not undergo a monotonic variation. A critical point, $C^*_{bub,crt}$, exists which satisfies the equation

$$C^*_{bub,crt}(t^*) = \frac{6}{6 + \dfrac{\Xi}{t^{*1/6}}} \tag{23}$$

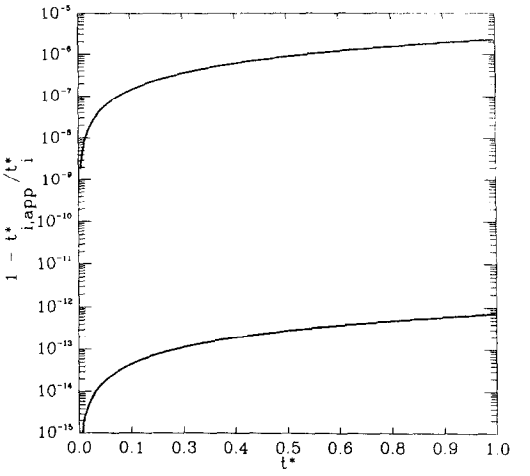

FIG. 3. Check of validity of approximation I presented as $(t_i^* - t_{i,app}^*)/t_i^*$ vs t^* for the volumetric flow rates of 5.0×10^{-4} $m^3\ s^{-1}$ (upper curve) and 5.0×10^{-6} $m^3\ s^{-1}$ (lower curve).

provided that equation (17) is recalled. Differentiating equation (17) twice with respect to t^*, and using equation (23), one gets

$$\left(\frac{d^2 C^*_{bub}}{dt^{*2}}\right)_{C^*_{bub} = C^*_{bub,crt}} = \frac{\Xi}{6t^{*2}(\Xi + 6t^{*1/6})} \tag{24}$$

which takes positive values at all times. Equation (23) is, therefore, a necessary and sufficient condition for a minimum.

The validity of the four mathematical approximations introduced previously was tested a posteriori via use of equation (20). The fractional error involved in the approximations can be depicted in Figs. 3–6 for two volumetric flow rates bounding the region of industrial interest.

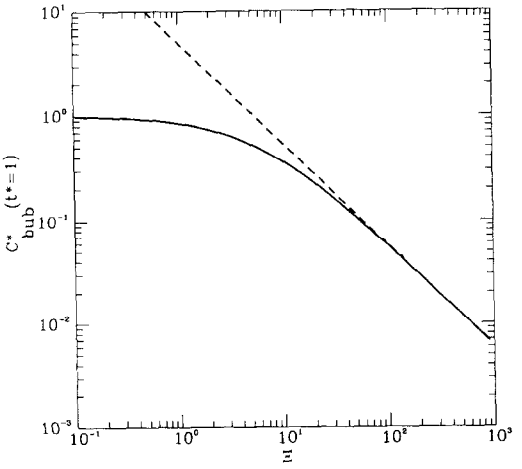

FIG. 2. Log–log plot of $C^*_{bub}(t^* = 1)$ vs Ξ (solid line). The asymptotic linear behaviour at high Ξ is represented by the dashed line.

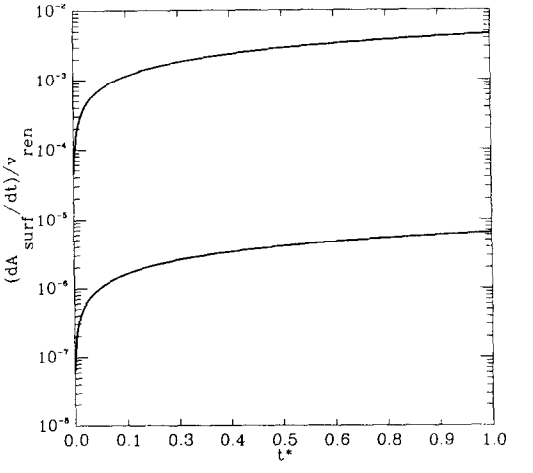

FIG. 4. Check of validity of approximation II presented as $(dA_{surf}/dt)/v_{ren}$ vs t^* for the volumetric flow rates of 5.0×10^{-4} $m^3\ s^{-1}$ (upper curve) and 5.0×10^{-6} $m^3\ s^{-1}$ (lower curve).

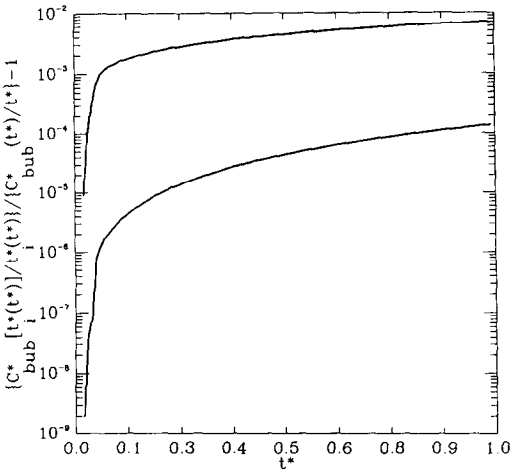

FIG. 5. Check of validity of approximation III presented as $[C^*_{bub}(t_i^*)/t_i^* - C^*_{bub}(t^*)/t^*]/[C^*_{bub}(t^*)/t^*]$ vs t^* for the volumetric flow rates of 5.0×10^{-4} m^3 s^{-1} (upper curve) and 5.0×10^{-6} m^3 s^{-1} (lower curve).

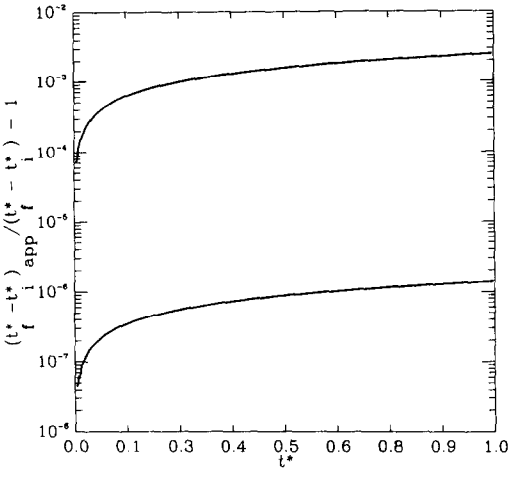

FIG. 6. Check of validity of approximation IV presented as $[(t_f^* - t_i^*)_{app} - (t_f^* - t_i^*)]/(t_f^* - t_i^*)$ vs t^* for the volumetric flow rates of 5.0×10^{-6} m^3 s^{-1} (upper curve) and 5.0×10^{-4} m^3 s^{-1} (lower curve).

3. STATISTICAL ANALYSIS

The adequacy of the jet stream model was tested by fitting it to 11 experimental points of C^*_{bub} vs Q_{gas} for the system NH_3/air–HCl/water [3]. In these experiments a nozzle with $R_{noz} = 5.0 \times 10^{-3}$ m was employed. The values used for the relevant physical properties are as follows: $\mathscr{D}_{gas} = 2.2 \times 10^{-5}$ m^2 s^{-1} [3], $\mu_{gas} = 1.813 \times 10^{-5}$ kg m^{-1} s^{-1} [16], and $\rho_{gas} = 1.189$ kg m^{-3}. The value used for the physical constant is $g = 9.8$ m s^{-2}.

The derivative of the expectation function with respect to either parameter depends in turn on both parameters, so non-linear regression analysis was employed in the search for the best estimates of the parameters. The likelihood function of the parameters given the observed values was assumed to be maximized with respect to the parameters when the residual sum of squares is a minimum (for assumptions underlying validity thereof, see, e.g. ref. [28]). The non-linear least squares fit was performed via a numerical algorithm implemented in the S language [42] using a Gauss–Newton linear approximation to the expectation function [28] with local corrections on the size of the increment [29, 30] introduced for increased robustness.

Since the jet stream model is transformably linear, the initial estimates for parameters Φ and ξ were obtained by linear regression [31] after applying logarithms to both sides of the approximate expectation function (i.e. equation (22)). For the one-parameter, partial model based on a Poiseuille-type law for the dependence of the pressure drop on the inlet velocity (i.e. $\xi = 1$) a linear regression analysis with no slope was implemented to get the starting estimate. Once in possession of these initial estimates, the non-linear regression algorithm proceeds to convergence under a very narrow tolerance in a few iterations. The starting and final best estimates, their standard errors, and t-ratios for both the full and the partial models, as well as the correlation matrix for the full model are tabulated in Table 2.

Since there is a well justified expectation function for the response, if the data should be transformed to induce constant variance then the same transformation should be applied to the expectation function to preserve the fundamental relationship [32]. Using power transformations of the response as suggested by Box and Cox [33] within the usual range for the exponent λ, the best estimate for λ was calculated using the maximum log-likelihood theory with estimates for the parameters as obtained from non-linear regression. The plot of the optimum log-likelihood function against λ is available as Fig. 7, coupled with an approximate confidence interval [34, 35].

In order to decide whether the simpler nested model (i.e. the jet stream model with $\xi = 1$) can fit the data set adequately, an extra sum of squares analysis was implemented with results summarized in Table 3.

The studentized residuals [28] for the full model using the best estimates obtained from non-linear regression analysis were plotted vs the predictor variable, and vs the estimated response in Fig. 8. The studentized residuals are also represented as a quantile–quantile plot in Fig. 9.

The discrete data employed in the non-linear least squares fit are represented in Fig. 10. The continuous predicted change in C^*_{bub} with Q_{gas} is overlaid in this picture as well as the results obtained from the model proposed by Rocha and Guedes de Carvalho [3] to explain their experimental results.

Linear approximation inference intervals for each experimental point and linear approximation inference bands for the expected response [28] at the 0.1% significance level are denoted as Fig. 11. The joint parameter inference regions represented in Fig. 12

Table 2. Starting estimates using linear regression, best estimates using non-linear regression, corresponding standard errors, t-ratios and correlation matrix based on the linear approximation about the optimum for both the complete and partial jet stream models

Model	Parameter	Starting estimate	Best estimate	Standard error	t-Ratio	Correlation matrix
Full	Φ	1.7711×10^{-3}	1.7682×10^{-3}	6.0425×10^{-5}	29.26	1.0000 0.5127
	ξ	1.20833	1.20736	2.8183×10^{-2}	42.84	0.5127 1.0000
Partial	Φ	2.1683×10^{-3}	1.6185×10^{-3}	1.3171×10^{-4}	12.29	

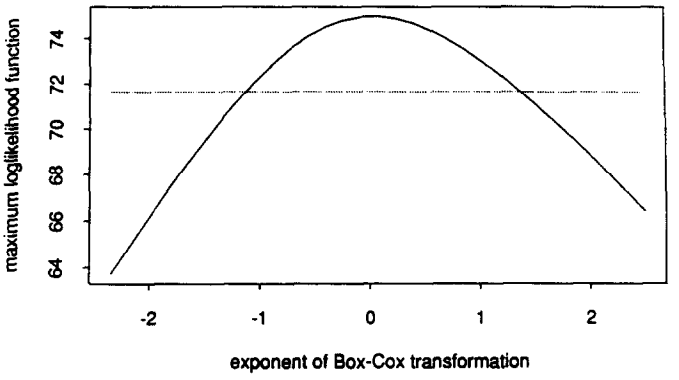

FIG. 7. Plot of the log-likelihood function vs λ for the best fit to the experimental data for each λ (solid curve). The 99% confidence interval is enclosed by the intercepts of the dashed line with the solid curve.

were obtained using both the likelihood theory and the Bayesian approach [28] with uninformative independent priors for the parameters and the variance [36].

The selection of the parameter form in the jet stream model was dictated by the steps of the mathematical derivation. A number of alternative forms for the parameters can be devised, nevertheless. One of the two obvious reparametrizations (with parameters ϕ and φ) enforces the physical constraint that C^*_{bub} must monotonically increase with Q_{gas} (as found in practice [3]), and ensures that the proportionality constant is always positive. The alternative reparametrization (with parameters v and θ) allows convergence problems to be relaxed because the suggested restatement of the jet stream model makes it conditionally linear in v [28]; this feature can be used in more efficient formulations of the Gauss–Newton approach [37].

The measure of the nonlinearity of the jet stream model was done by investigating the second-order derivatives of the expectation function [38–40]. The relative curvature array [28] accounted for by the parameter effect nonlinearity for the original complete jet stream model, and the transformed model after each one of the foregoing reparametrizations, are tabulated in Table 4. The parameter effect and intrinsic root mean square curvatures [40] corrected by the multiplicative factor $\sqrt{F}$ are presented in Table 5.

The estimates for the parameters can be refined by carefully designing extra experiments according to Wald's determinant criterion [41]. The D-profile within the range where the experimental data were obtained is depicted in Fig. 13.

4. DISCUSSION

The gaseous bubbles generated at the tip of the submerged nozzle possess an ellipsoidal shape [3] rather than a spherical shape as assumed in the development of the model. However, the difference in surface area between the two geometries for the same bubble volume does not introduce major changes in the predicted values of the mass transfer rates because the forced surface renewal is of much less importance than the natural surface renewal for most applications (see approximation II). If full advantage is to be taken

Table 3. Extra sum of squares analysis for the partial and full jet stream model

Source	Sum of squares	Degrees of freedom	Mean square	F-Ratio	Associated probability (%)
Extra parameter	1.381×10^{-4}	1	1.381×10^{-4}	66.883	0.002
Full model	1.859×10^{-5}	9	2.065×10^{-6}		
Partial model	1.567×10^{-4}	10			

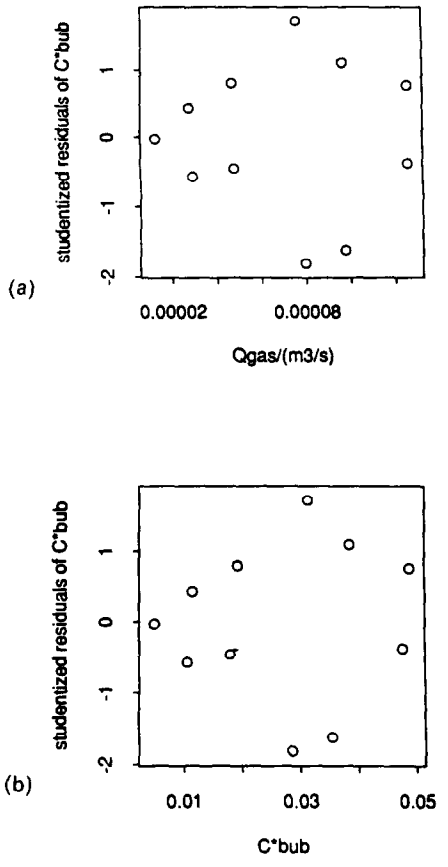

FIG. 8. Studentized residuals for the full jet stream model using the best parameter estimates obtained from non-linear least squares plotted vs the predictor variable (a), and vs the estimated response (b).

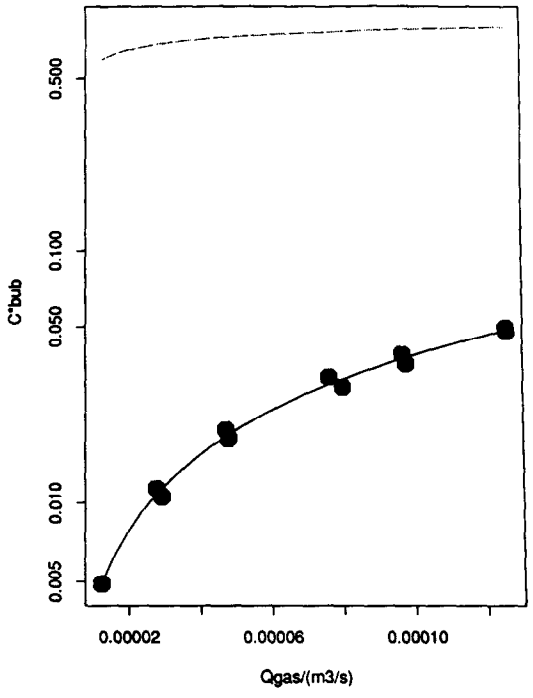

FIG. 10. Semi-log plot of the experimental data employed in the non-linear least squares fit (filled octagons), overlaid with the predicted values for C^*_{bub} using the complete jet stream model (solid line) and the predictions using the theoretical model proposed elsewhere [3] (dashed line).

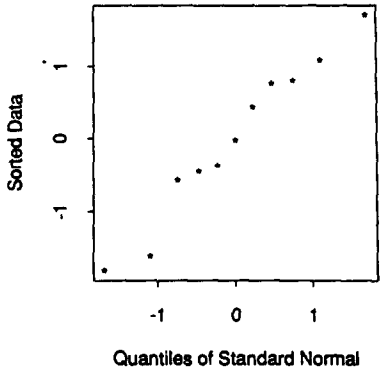

FIG. 9. Sorted studentized residuals for the full jet stream model using the best parameter estimates obtained from non-linear least squares plotted vs the quantiles of a standard normal distribution.

from the enhanced rates of solute removal during bubble formation, then low heights of liquid are required and hence isobaric conditions apply throughout as stated in assumption (ii). For common industrial applications, the solute to be removed exists at very dilute levels (say, below 5%) because this compound is an impurity or a by-product rather than the desired product of a process; hence, assumption (iii) holds. The degree of circulation within the bubble is usually very high due to the narrow nozzle opening coupled with the relatively short size of the bubble formed; therefore, the development of significant concentration gradients in the bulk of the bubble is improbable (cf. assumption (iv)). Assumption (v) is a direct consequence of the strong interaction of the gaseous jet with the existing bubble arising from high linear velocities at the nozzle opening. The region where new gas elements are more likely to become a portion of the bubble surface layer corresponds to the vicinity of the intercept of the jet axis with the bubble surface as emphasized by assumption (vi) because the largest velocity is expected at this point. The bubble is considered to form exactly around the axis of symmetry of the nozzle tip and to grow from the nozzle tip with no coalescence between the bulk gas and the nozzle material. This implies that the centre of mass of the bubble actually rises in space as more gas is admitted through the nozzle. If the non-slip condition is satisfied at the gas/liquid interface, then the gas elements on the surface change positions according to a toroidal-like path with respect to the axis with the origin located at the centre of mass of the bubble, and

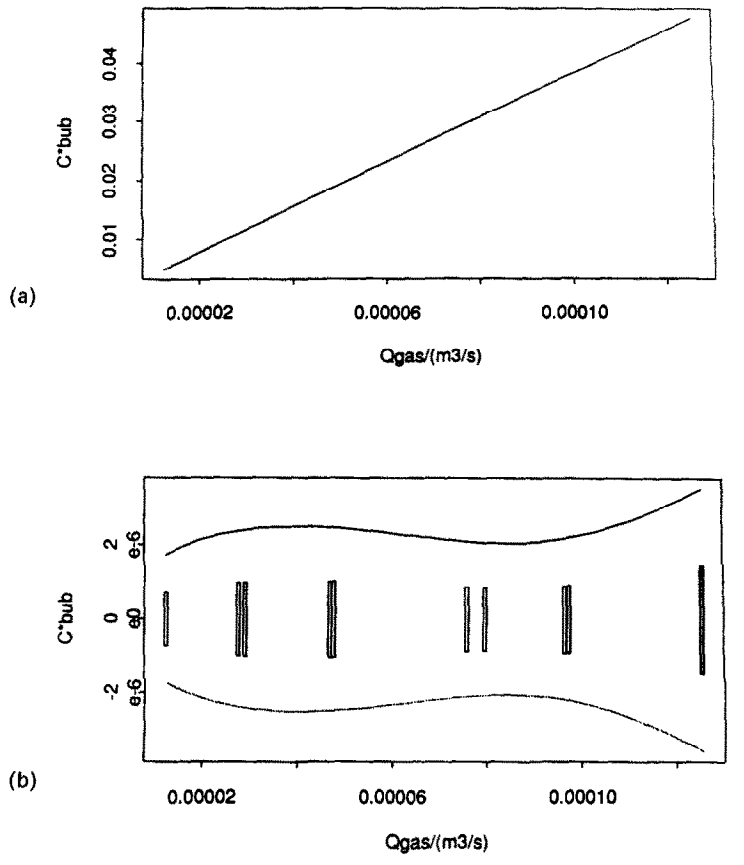

FIG. 11. Linear plot of the expected response for C^*_{bub} (a), coupled with the linear approximation inference intervals for each experimental point (b, open rectangles) and the linear approximation inference bands for the expected response (b, solid lines) at the 0.1% significance level.

so assumption (vii) has a physically reasonable basis. This phenomenon is the bubble-growth equivalent of the bubble-rising plug-flow suggested elsewhere [16]. In the reasoning leading to the jet stream model, one only transformed the above rate of surface displacement (static conception) into a rate of surface renewal (dynamic conception), which changes with time according to a postulated mathematical form. Assumption (viii) is a straightforward consequence of the dynamic nature of the model reported. The difference between solute concentration of adjacent gas elements on the surface of the bubble is very small compared with the difference in concentration between the bulk of the bubble (from which these gas elements were generated) and the gas/liquid interface (null solute concentration), so assumption (ix) is justified. The gas phase often consists of a solute dissolved in air, whereas the liquid phase often involves an aqueous solution of reactant. All air components are sparingly soluble in water; if the inlet stream is, in addition, saturated with humidity, then all components except the solute are stagnant (cf. assumption (x)). Assumption (xi) is explained on the grounds that the gas elements keep their identity while being displaced along the bubble surface, and that their residence time on the surface is very small (as expected from large values of Φ). In spite of the many assumptions considered in the derivation of the jet stream model, the results from the model are of practical relevance because the fit of only two parameters is required and because a functional relationship of the amounts of solute removed on physically measurable quantities is obtained.

The power dependence of Θ on $U(x = 0, \zeta = 0)$ with a positive exponent (see equation (7)) accommodates two fundamental physical constraints on the hydrodynamic pattern within the bubble: (i) at very large inlet velocities, the bulk of the gas undergoes complete micromixing, so the width of the jet is virtually infinite at all longitudinal locations; and (ii) at very low inlet velocities, the width of the jet reduces to zero, irrespective of the longitudinal location within the bubble. Although this Fanning factor vs Reynolds type of functionality was tentatively assumed, it turns out to be a very reasonable approximation because the best estimate for ξ is around 1.2, a value lying between 1 (stable laminar flow) and 7/4 (from the Blasius formula for the turbulent regime) [46].

The general approximate solution of equations (1) and (2) (i.e. equation (20)) is not required from an

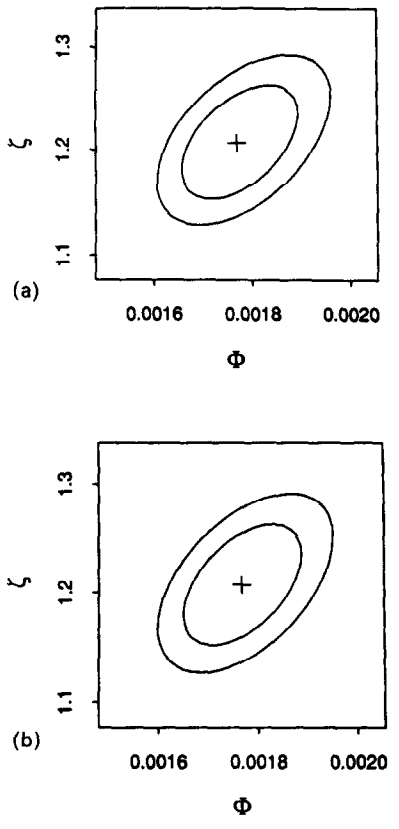

FIG. 12. Joint parameter inference regions at the 20% (inner ellipses) and 5% (outer ellipses) significance level using the likelihood theory (a) and the Bayesian approach (b). The best estimates of the parameters are denoted by a cross (+).

engineering point of view because the operating range of industrial interest requires that Ξ be very large: this conclusion is possible a priori on the basis of Fig. 2 coupled to the fact that the values observed for the fractional removal are usually very high [3]. This result is expected because the reciprocal square-root dependence of the average molar rate of stripping on the exposure time resulting from the general principles of the penetration theory tends to damp the transport process very rapidly yielding a first-order, exponential dependence of the solute concentration on Ξ.

Table 4. Relative curvature matrices for the parameters in the original model, and in the models obtained after the suggested reparametrizations

Parameter	Relative curvature matrix	
Φ	−0.00004	−0.00002 −0.00003
ξ	0.00000	−0.00002 −0.00003
ϕ	−0.00002	−0.00000 −0.00003
φ	0.00000	−0.00002 −0.00005
ν	0.00000	0.00001 −0.00001
θ	0.00000	−0.00001 −0.00003

The four mathematical approximations were tested a posteriori for two limiting flow rates of the dispersed phase over a time range comprising the life span of the bubble using the approximate analytical solution as given by equation (20). In all cases relative errors were considered rather than absolute errors because the physical properties of the bubble may undergo order of magnitude variations during bubble growth (namely, the dimensionless solute concentration drops from unity down to less than 0.05 for most cases of interest, and the dimensionless time interval spent by a gas element on the surface of the bubble increases from zero to 10^{-4}). The error involved in all approximations increases very rapidly from zero during the time immediately following bubble birth, but then tends to an asymptotically constant value as the time of bubble release is approached. For approximations I and IV this behaviour is expected on the basis of the decrease in goodness of the linear approach based on the Taylor series expansion. The behaviour of approximation II is due to the decrease of v_{ren} relative to dA_{surf}/dt as time elapses resulting from the t^{*-1} and $t^{*-1/3}$ functional dependencies, respectively. The pattern for approximation III can be explained as follows: (i) at bubble birth, t_f^* and t_i^* are virtually the same, so the relative error expressed as $[C^*_{bub}(t_i^*)/t_i^* - C^*_{bub}(t_f^*)/t_f^*]/C^*_{bub}(t_f^*)/t_f^*$ is zero; (ii) at very short times, the concentration of solute decreases rapidly and $(t_f^* - t_i^*)$ increases steadily, so the relative error undergoes a fast increase; (iii) after the minimum for the concentration of solute is reached the change in concentration with time becomes much shallower and a monotonically increasing function, so the relative error tends to be damped down. All approximations are well below the level of 1% relative error. This relative error is acceptable because it lies below the error associated with the determination of the final concentrations immediately after the bubble is released (see practical determination of $C^*_{bub}(t^* = 1)$ [3]).

Two characteristic time scales can be devised in the mass transfer process: the time scale for the change in concentration of the core of the bubble, and the time scale for the diffusional process occurring within the shell of the bubble. The mathematical formulation of the postulated model was extremely facilitated because these two processes could be decoupled due to validity of approximation III.

The theoretical expressions derived from first principles employed by Rocha and Guedes de Carvalho [3] lead to predictions of the fractional solute removal more than one order of magnitude below the experimental results obtained. The double surface-renewal model suggested by Malcata [14] is able to decrease the relative error of the predictions, although the fit

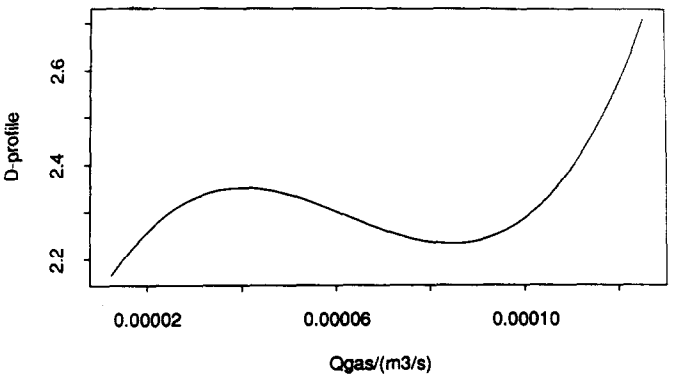

FIG. 13. D-Profile plotted vs the predictor variable within the range of the experimental results available.

is still bad. The improvement more recently reported by the same researcher [15] involving the inclusion of an adjustable parameter is able to bring the theoretical results closer to the experimental ones, although a trend in the sign of the residuals exists as the volumetric flow rate is monotonically changed. All these problems are overcome with the jet stream model, which is able to accurately predict the observed results with two adjustable parameters to which physical significance can be ascribed.

The t-ratios for both parameters in the complete model are well above unity, so the null hypothesis is rejected for both parameters. Furthermore, inspection of Table 2 allows one to find that the parameters are not excessively correlated for the full model (i.e. correlations are well below 0.99), so overparametrization is not likely to have occurred.

In order to decide if a simpler model nested in the full jet stream model can fit the data set adequately, a likelihood ratio test was used as in the linear case [31, 34]. Since the distribution of the mean square ratio is only affected by the intrinsic nonlinearity [28], and since this type of nonlinearity is very small in our case (see Table 5), then inspection of Table 3 allows one to assert that there is a 99.998% chance that parameter ξ be significant for the fit. Therefore, one should retain ξ as an adjustable parameter, and so accept the full model.

The non-linear estimation procedure employed converged to a minimum value of the residual sum of squares. Since no replications were reported as such for the experimental data available [3], the assessment of the validity of the underlying assumption of constant variance of the dependent variable over the range of interest of the predictor variable was obtained via a suitable transformation of the response [29]. The value for λ that maximizes the likelihood function is around $\lambda = 0$. The null hypothesis of having no transformation of the data is accepted at the 1% significance level, so the assumption of constancy of variance for the disturbances can be taken as valid for the model in its native form.

Table 5. Analysis of root mean square curvature corrected at the 5% significance level due to parameter effects nonlinearity and intrinsic nonlinearity

Source of nonlinearity	Corrected root mean square curvature
Parameter	8.8287×10^{-5}
Intrinsic	3.3247×10^{-5}

The results from the check of the adequacy of the model using a plot of the studentized residuals vs the predictor variables [43–44] can be depicted in Fig. 8(a): no strong relationship is revealed between the residuals and the predictor, so all effects due to such a variable seem to have been accounted for in the model. Systematic bias in the behaviour of disturbances or significant outliers is not observed for the residuals in Fig. 8(b), so the expectation function seems adequate. This fact can be confirmed by observation of the plot of the data overlaid with the plot of the expectation function (Fig. 10): the fit is very good, so convergence took place towards a global minimum in the residual sum of squares.

The quantile–quantile plot of the studentized residuals vs a normal distribution does not deviate appreciably from a straight line, thus suggesting appropriateness of the normality assumption [44] (see Fig. 9): the criterion of the least squares can, thus, be applied. Some of the observed variability can be explained due to the nature of the plot [45]. No real outliers can be found in the aforementioned plot.

The 99.9% inference intervals and inference bands for the predictions are extremely narrow (see Fig. 11) as a consequence of the very low variability of the data about the predictions. The joint parameter inference regions share basically the same location and shape for the two theoretical explanations (see Fig. 12). Moreover, the contours are almost perfect ellipses with ratio of major and minor axis close to unity thus indicating small correlation of the parameter estimates (cf. Table 2). Larger values for parameter Φ lead to larger values for parameter ξ.

The relative curvature measures listed in Table 4

for the parameter effect nonlinearity show that (i) the assumption of planarity of the jet stream model in its native parametric form is a very good approximation [28], and that (ii) although each of the two reparametrizations listed improves the linearity of the model, the change in the parameter effects is slight. The square root of the average over all directions of the squared curvature is tabulated in Table 5 after having been multiplied by the square root of $F(\nu_1 = 2, \nu_2 = 9; \alpha = 5\%)$. Both root mean square curvatures (RMSC) are much less than the curvature of the 95% confidence disk, so the deviation of the expectation surface with radius 1/RMSC from the tangent plane at a distance $\sqrt{F}$ from the tangent point is only a small fraction of 1% of the radius of the confidence disk.

Once in possession of estimates for the relevant parameters, the main goal of further experimentation should be how to refine these estimates. This refinement may also serve as a double check of the physical assumptions involved in the theoretical derivation: obvious limitations of the experimental data included in the analysis arise from the use of a single system and temperature (i.e. constant values for ρ_{gas}, μ_{gas}, and $\mathscr{D}_{gas}$), as well as the use of a single type of nozzle (i.e. same R_{noz}). In terms of Q_{gas}, a logical choice is to design experiments at volumetric flow rates such that the volume of the joint inference region [28], or the determinant of the product of the transpose of the derivative matrix and the derivative matrix itself [47], is minimized. Inspecting Fig. 13, one finds that the best design point should correspond to a volumetric flow rate as high as possible.

Acknowledgements—The author is indebted to Prof. D. M. Bates, c/o Department of Statistics, University of Wisconsin–Madison (U.S.A.), for his permission to use some software facilities of his authorship available in the S environment and for his critical review of some particularly complex mathematical topics relevant for the reported research.

REFERENCES

1. P. V. Danckwerts, *Gas–Liquid Reactions*. McGraw-Hill, New York (1970).
2. R. H. Perry, D. W. Green and J. O. Maloney (Editors), *Perry's Chemical Engineers' Handbook*. McGraw-Hill, New York (1984).
3. F. A. N. Rocha and J. R. Guedes de Carvalho, Absorption during gas injection through a submerged nozzle—Part I: gas side and liquid side transfer coefficients, *Chem. Engng Res. Des.* **62,** 303–314 (1984).
4. T. K. Sherwood and R. L. Pigford, *Absorption and Extraction*. McGraw-Hill, New York (1952).
5. W. E. Stewart, J. B. Angelo and E. N. Lightfoot, Forced convection in three-dimensional flows: II—asymptotic solutions for mobile interfaces, *A.I.Ch.E. Jl* **16,** 771–786 (1970).
6. J. B. Angelo, E. N. Lightfoot and D. W. Howard, Generalization of the penetration theory for surface stretch: application to forming and oscillating drops, *A.I.Ch.E. Jl* **12,** 751–760 (1966).
7. D. W. Howard and E. N. Lightfoot, Mass transfer to falling films: part I—application of the surface stretch model to uniform wave motion, *A.I.Ch.E. Jl* **14,** 458–467 (1968).
8. G. E. Fortescue and J. R. A. Pearson, On gas absorption into a turbulent liquid, *Chem. Engng Sci.* **22,** 1163–1176 (1967).
9. R. B. Bird, W. E. Stewart, E. N. Lightfoot and T. W. Chapman, *Lectures in Transport Phenomena*. American Institute of Chemical Engineers, New York (1969).
10. V. G. Levitch, *Physicochemical Hydrodynamics*. Prentice-Hall, Englewood Cliffs, New Jersey (1962).
11. T. K. Sherwood, R. L. Pigford and C. R. Wilke, *Mass Transfer*. McGraw-Hill, New York (1975).
12. W. J. Beek and H. Kramers, Mass transfer with a change in interfacial area, *Chem. Engng Sci.* **16,** 909–921 (1962).
13. P. H. Calderbank and R. P. Patra, Mass transfer in the liquid phase during the formation of bubbles, *Chem. Engng Sci.* **21,** 719–721 (1966).
14. F. X. Malcata, Double surface-renewal model for the prediction of mass transfer rates during bubble formation with instantaneous reaction on the liquid side, *Int. J. Heat Mass Transfer* **31,** 567–575 (1988).
15. F. X. Malcata, The prediction of mass transfer rates during bubble growth in the presence of an instantaneous reaction on the liquid side, *Chem. Engng Sci.* **45,** 565–568 (1990).
16. R. B. Bird, W. E. Stewart and E. N. Lightfoot, *Transport Phenomena*. Wiley, New York (1960).
17. R. Higbie, The rate of absorption of a pure gas into a still liquid during short periods of time, *Trans. A.I.Ch.E.* **31,** 365–389 (1935).
18. P. V. Danckwerts, *Gas–Liquid Reactions*. McGraw-Hill, New York (1970).
19. H. Schlichting, *Boundary Layer Theory*. Pergamon Press, London (1955).
20. M. Z. Krzywoblocki, On steady, laminar round jets in compressible viscous gases far behind the mouth, *Oesterr. Ing. Arch.* **3,** 404–408 (1949).
21. H. Schlichting, Laminare Strahlausbreitung, *Z. Angew. Math. Mech.* **13,** 260–265 (1933).
22. J. F. Davidson and B. O. G. Schüller, Bubble formation at an orifice in a viscous liquid, *Trans. Instn Chem. Engrs* **38,** 335–342 (1960).
23. F. Homann, Der Einfluß großer Zähigkeit bei der Strömung um den Zylinder und um die Kugel, *Z. Angew. Math. Mech.* **16,** 153 (1936).
24. L. Prandtl, Über Flüssigkeitsbewegung bei sehr kleiner Reibung, *Proc. III Int. Math. Congr.*, Heidelberg (1904).
25. J. A. W. Bye and J. Schenk, Heat transfer in laminar flow between two parallel plates, *Appl. Scient. Res.* **A3,** 308–316 (1952).
26. J. A. Prins, J. Mulder and J. Schenk, Heat transfer in laminar flow between parallel plates, *Appl. Scient. Res.* **A2,** 431–438 (1951).
27. G. Stephenson, *Mathematical Methods for Science Students*. Longman, London (1973).
28. D. M. Bates and D. G. Watts, *Nonlinear Regression Analysis and its Applications*. Wiley, New York (1988).
29. G. E. P. Box, Fitting empirical data, *Ann. N.Y. Acad. Sci.* **86,** 792–816 (1960).
30. H. O. Hartley, The modified Gauss–Newton method for the fitting of non-linear regression functions by least squares, *Technometrics* **3,** 269–280 (1961).
31. D. A. Ratkowski, *Nonlinear Regression Modelling: a Unified Practical Approach*. Marcel Dekker, New York (1983).
32. R. J. Carrol and D. Ruppert, Power transformation when fitting theoretical models to data, *J. Am. Statist. Ass.* **79,** 321–328 (1984).
33. G. E. P. Box and D. R. Cox, An analysis of transformations, *J. R. Statist. Soc.* **B26,** 211–243 (1964).
34. N. R. Draper and H. Smith, *Applied Regression Analysis*. Wiley, New York (1981).
35. A. C. Atkinson, Testing transformations to normality, *J. R. Statist. Soc.* **B35,** 473–479 (1973).
36. G. E. P. Box and G. C. Tiao, *Bayesian Inference in*

Statistical Analysis. Addison-Wesley, Reading, Massachusetts (1973).
37. G. H. Golub and V. Pereyra, The differentiation of pseudo-inverses and non-linear least squares problems whose variables separate, *J. SIAM* **10,** 413–432 (1973).
38. D. M. Bates, Curvature measures of nonlinearity, Ph.D. thesis, Queen's University at Kingston, Canada (1978).
39. D. M. Bates and D. G. Watts, Relative curvature measures of nonlinearity (with discussion), *J. R. Statist. Soc.* **B42,** 1–25 (1980).
40. E. M. L. Beale, Confidence regions in nonlinear estimation (with discussion), *J. R. Statist. Soc.* **B22,** 41–88 (1960).
41. A. Wald, On the efficient design of statistical investigations, *Ann. Math. Statist.* **14,** 134–140 (1943).
42. R. A. Becker, J. M. Chambers and A. R. Wilks, *The New S Language*. Wadsworth & Brooks/Cole Advanced Books & Software, Pacific Grove, California (1988).
43. B. L. Joiner, Lurking variables—some examples, *Am. Statistician* **35,** 227–233 (1981).
44. J. M. Chambers, W. S. Cleveland, B. Kleiner and P. A. Tukey, *Graphical Methods for Data Analysis*. Wadsworth & Brooks, Belmont, California (1983).
45. C. Daniel and F. S. Wood, *Fitting Equations to Data*. Wiley, New York (1980).
46. W. L. McCabe and J. C. Smith, *Unit Operations of Chemical Engineering*. McGraw-Hill, New York (1954).
47. G. E. P. Box and H. L. Lucas, Design of experiments in non-linear situations, *Biometrika* **46,** 77–90 (1959).

SIMULATION PAR UN MODELE DE JET DU COMPORTEMENT DU TRANSFERT DE MASSE DE BULLES INDIVIDUELLES DE GAZ EN REACTION CHIMIQUE RAPIDE

Résumé—On simule par un modèle à deux paramètres le transfert de masse de soluté d'un mélange gazeux dilué pendant la formation de la bulle au sommet d'une tuyère immergée, en présence d'une réaction chimique instantanée du côté du liquide. Ce modèle mécaniste est développé à partir du bilan général de masse du soluté en introduisant une nombre d'hypothèses raisonnables sur le plan physique, avec couplage à des approximations mathématiques contrôlées. En utilisant des données expérimentales, l'estimation des paramètres est faite et une analyse statistique de leur signification est présentée. L'expérience est prédite beaucoup mieux que par d'autres modèles théoriques. L'analyse présentée est utile pour la conception préliminaire d'unités industrielles parce que la plupart de l'enlèvement de soluté se fait pendant la croissance de la bulle.

SIMULATION DES STOFFÜBERGANGS IN EINZELNE GASBLASEN BEI DER REKTIFIKATION

Zusammenfassung—Es wird der Stofftransport in einem Gemisch aus dünnem Gas bei der Blasenbildung an der Mündung einer überfluteten Düse mit Hilfe eines Zweiparametermodells simuliert, wobei auf der Flüssigkeitsseite eine sofortige chemische Reaktion auftritt. Dieses mechanistische Modell wird aus der allgemeinen Stoffbilanz entwickelt, wobei eine Anzahl physikalisch sinnvoller Annahmen und sorgfältig überprüfter mathematischer Näherungen eingeführt wird. Mit Hilfe fremder Daten werden die Parameter ermittelt und eine statistische Analyse ihrer Bedeutung vorgelegt. Experimentelle Ergebnisse können wesentlich besser wiedergegeben werden als mit anderen theoretischen Modellen. Die analytische Untersuchung ist nützlich für die Erstauslegung industrieller Blasensäulen, weil der wesentliche Stoffübergang während des Blasenwachstums auftritt.

МОДЕЛИРОВАНИЕ МАССООБМЕНА ОТДЕЛЬНЫХ ПУЗЫРЬКОВ ГАЗА ПРИ ИХ БЫСТРОМ ХИМИЧЕСКОМ ВЫТАЛКИВАНИИ С ИСПОЛЬЗОВАНИЕМ МОДЕЛИ СТРУЙНОГО ТЕЧЕНИЯ

Аннотация—На основе двухпараметрической модели исследуется массоперенос растворенного вещества из разбавленной газовой смеси в процессе образования пузырьков у конца погруженного сопла при мгновенной химической реакции в жидкости. Предложенная механистическая модель разработана на основе общего массового баланса растворенного вещества при большом числе физически оправданных допущений, связанных с тщательно обоснованными математическими приближениями. С использованием опубликованных данных найдены параметрические оценки, и представлен статистический анализ их роли. Экспериментальные данные этой моделью предсказаны намного лучше, чем в случае применения других теоретических моделей. Предложенный анализ может использоваться для предварительного расчета промышленных баллонов для разбрызгивания веществ, так как удаление растворенного вещества происходит преимущественно в процессе роста пузырьков.